Article

Opening Size Effects on Airflow Pattern and Airflow Rate of a Naturally Ventilated Dairy Building—A CFD Study

Chayan Kumer Saha [1,2,*], **Qianying Yi** [1], **David Janke** [1], **Sabrina Hempel** [1], **Barbara Amon** [3,4] **and Thomas Amon** [1,5,*]

1 Department of Engineering for Livestock Management, Leibniz Institute for Agricultural Engineering and Bioeconomy (ATB), Max-Eyth-Allee 100, 14469 Potsdam, Germany; QYi@atb-potsdam.de (Q.Y.); djanke@atb-potsdam.de (D.J.); shempel@atb-potsdam.de (S.H.)

2 Department of Farm Power and Machinery, Bangladesh Agricultural University, Mymensingh-2202, Bangladesh

3 Department of Technology Assessment and Substance Cycles, Leibniz Institute for Agricultural Engineering and Bioeconomy (ATB), Max-Eyth-Allee 100, 14469 Potsdam, Germany; bamon@atb-potsdam.de

4 Faculty of Civil Engineering, Architecture and Environmental Engineering, University of ZielonaGóra, ul.Licealna 9, 65–762 ZielonaGóra, Poland

5 Institute of Animal Hygiene and Environmental Health, Department of Veterinary Medicine, Free University of Berlin, Robert-von-Ostertag-Str. 7–13, 14163 Berlin, Germany

* Correspondence: cksaha@bau.edu.bd (C.K.S.); tamon@atb-potsdam.de (T.A.)

check for updates

Abstract: Airflow inside naturally ventilated dairy (NVD) buildings is highly variable and difficult to understand due to the lack of precious measuring techniques with the existing methods. Computational fluid dynamics (CFD) was applied to investigate the effect of different seasonal opening combinations of an NVD building on airflow patterns and airflow rate inside the NVD building as an alternative to full scale and scale model experiments. ANSYS 2019R2 was used for creating model geometry, meshing, and simulation. Eight ventilation opening combinations and 10 different reference air velocities were used for the series of simulation. The data measured in a large boundary layer wind tunnel using a 1:100 scale model of the NVD building was used for CFD model validation. The results show that CFD using standard k-ε turbulence model was capable of simulating airflow in and outside of the NVD building. Airflow patterns were different for different opening scenarios at the same external wind speed, which may affect cow comfort and gaseous emissions. Guiding inlet air by controlling openings may ensure animal comfort and minimize emissions. Non-isothermal and transient simulations of NVD buildings should be carried out for better understanding of airflow patterns.

Keywords: Airflow; ventilation openings; CFD; natural ventilation; cow barns

1. Introduction

Air exchange in livestock buildings is very essential for creating a comfortable environment with satisfactory indoor air quality. Ventilation air is also a medium of transporting pollutants (i.e., gas, odor, and dust) from livestock buildings [1] which adversely affect animals, workers, neighbors, and the environment [2]. It is essential to have suitable tools to understand airflow characteristics and predict ventilation performance in buildings for regulating the indoor air parameters and controlling emissions.

The natural ventilation system with large side wall openings and a roof opening is commonly used in dairy cow barns of temperate climate regions [3]. Hence, atmospheric influences under continuously

changing conditions [4] (such as outdoor temperature, wind speed and wind direction, as well as its turbulence properties) influences the emission from naturally ventilated dairy (NVD) barns directly. Milk production and milk quality are badly affected by stale air. However, animal activity changes in response to heat stress [5] and insufficient fresh air [6].

The design and performance of the ventilation system, including ventilation openings strategies, maintain desired environmental conditions in intensive livestock production systems. Ventilation in an NVD building is the result of pressure differences created by either temperature differences (thermal buoyancy), wind on the building or combinations of the two. As a consequence, the indoor environmental parameters (temperature, gases, and humidity) are governed by airflow patterns. The essential link between the outdoor environment and the buildings microclimate is formed by the airflow patterns including air velocities and turbulence intensity; thus, an understanding of the principles of air motion is necessary in order to provide optimum air flow, air exchange rate (AER), and the proper airflow distribution patterns to meet the needs of the livestock and environment.

The major problem of natural ventilation is the lack of precise, continuous, and online measuring and control techniques for ventilation rate [7]. Ventilation rates and the emission streams from naturally ventilated buildings have been measured and calculated, respectively by applying different measuring techniques (e.g., heat balance [8], CO_2 balance [9], moisture balance [10], hot wire anemometer [11], tracer gas [12], etc.). Depending on the different methods and techniques, imperfect mixing of tracer gases and lack of representative sampling errors give errors up to 100% [7,13]. Recently, wind tunnel investigations using 1:40 scale models of a naturally ventilated dairy building were conducted for better understanding of opening effects on indoor airflow pattern and on the discharge coefficient, which is an important parameter in the airflow rate determination when using the orifice equation method [14,15]. However, wind tunnel experiments are expensive, labor intensive, and technically difficult, because extensive information on airflow characteristics in the space is needed and the number of points that can be measured is limited [13]. Thus, a model would be very helpful for predicting the airflow rates and airflow characteristics by using parameters easily measured or obtained from the available literature. For understanding airflow characteristics of NVD buildings, numerical simulation using computational fluid dynamics (CFD) could ideally complement full scale and scale model experiments [16,17].

Gebremedhin and Wu [18] investigated the flow around cows using CFD to investigate the heat and mass transfer phenomena coupled fur model to calculate sensible and latent heat losses from the skin surface of an actual cow in a forced ventilated enclosure of simple geometry. The total heat loss from an animal is highly dependent on both the animals' position and orientation to the flow field. Furthermore, a wall inlet which produce a ceiling air jet helped to create the most uniform environmental conditions in the building and minimized the large differences in animal heat loss [18]. Norton et al. [19] used CFD and a half scale experimental duopitch building for studying ventilation effectiveness of naturally ventilated livestock buildings under wind dominated conditions. They have found that the wind blowing normal to the building provided maximum ventilation homogeneity. CFD was also used to optimize the ventilation configuration of naturally ventilated livestock buildings for improved indoor environmental homogeneity and calf comfort [19]. In other studies, CFD technique was applied in NVD buildings for examining suitability of response surface methodology for ventilation rate calculation [20,21]. However, geometric structure and orientation of the buildings largely affects the airflow patterns inside the barn and emission behavior [22] and these were not systematically investigated in the above-mentioned studies. Typical NVD buildings located in temperate regions have large side wall openings. Numerical studies were conducted using a 1:40 scale model of an NVD building for understanding building configurations and wind condition effects on the discharge coefficient [17,20]. However, the studies did not provide the ventiation rate in different scenarios and did not include feeding alley and cow resting places. However, it is worthwhile to investigate air velocities and opening effects on air exchange rate, airflow patterns and inlet air jets in a different size of a scale model including feeding alley and resting places considering different air velocities and real

opening practices of commercial dairy farms in different seasons. Furthermore, it is very important to understand spatial characteristics of airflow inside barns from animal comfort aspects. At the same time, emissions might be reduced, and animal comfort can be improved by using appropriate sidewall opening strategies by controlling airflow rates and inlet air jets to the required ventilation rates in a full-scale livestock building. Constructing a model geometry of a NVD building at a different scale (1:100), and performing CFD simulation may provide useful information on airflow characteristics at the animal height and floor regions The simulation results may also provide information on emission reduction potentials by reducing the convective mass transfer from the active emitting surface and ensure the cow comfort. Therefore, this study was conducted using CFD to investigate the effect of different seasonal opening combinations of an NVD building on airflow patterns and airflow rate of the NVD building. The CFD simulation may lead to find optimal opening combinations in a season.

2. Materials and Methods

2.1. The Prototype NVD Building and Seasonal Practices

The naturally ventilated dairy building located in Dummerstorf, northeast Germany (217 km north-west Berlin, 54°1′0″N, 12°13′60″E, altitude 43 m) is considered for a scale model study in a Boundary Layer Wind Tunnel (BLWT) and CFD simulation. The full-scale dairy building is 96.15 m (length) × 34.2 m (width) (Figure 1a). The height of the sheet metal roof varies from 4.2 m at the sides to 10.73 m at the gable peak. The dairy building is equipped with long sidewall openings with adjustable curtains (polyethylene film, 1 mm). The building has leeward sided roof opening of 0.2 m height, space boards (11.5 cm width × 2.5 cm space) in the western side gable wall and the sheet metal wall in the eastern side. There are four doors (two doors 3.2 m × 4 m and two doors 3.2 m × 3 m) and one gate (4 m × 4.4 m) in each gable wall (Figure 1a). The gates and the doors are kept open normally except in very cold winter. Three general practices of sidewall openings are observed during different seasons and weather conditions. Side walls are 4.2 m high where middle part (2 m height) and bottom part (1.3 m height) of the side walls are open during summer (Figure 1b). The middle part of the side walls is kept open and bottom part is kept closed with the flexible curtains during early spring and autumn especially in chilling weather (Figure 1b). In the very cold weather in winter, side walls opening are kept closed (Figure 1c). The leeward roof opening is always kept open.

(**a**) NVD in summer

(**b**) early spring and autumn

Figure 1. *Cont.*

(**c**) winter

Figure 1. Sidewall opening practices of the naturally ventilated dairy (NVD) barn in Dummerstorf, Germany in different seasons, (**a**) in summer, (**b**) in early spring and autumn, and (**c**) in winter.

2.2. Wind Tunnel Experiments for CFD Model Validation

Before analyzing the airflow pattern, the CFD model validation is necessary to ensure adequate results [23]. This can be done best under constant boundary conditions; hence wind tunnel experiments are ideal for that purpose. In this study, boundary layer wind tunnel (BLWT) (ATB, Potsdam, Germany) at the Leibniz Institute for Agricultural Engineering and Bioeconomy (ATB) was used for data generation in constant environmental condition and model validation.

2.2.1. Description of the Wind Tunnel and a Scale Model of NVD Building

The experiments were carried out in a large BLWT at the ATB. The BLWT is 20 m long, 3 m wide and 2 m high with adjustable ceiling up to 0.25 m (Figure 2). The inlet of the BLWT is fitted with honeycombs (Sennur Camur, Bad Saeckingen, Germany) at the inlet nozzle and has a Prandtl tube sensor connected to a pressure transducer (MKS Baratron^R Type 120A, MKS Instruments, USA) near the inlet to measure the inlet velocity. The inflow section between inlet and test section had a length of approximately 10 m and was equipped with roughness elements of different heights to generate a turbulent boundary layer. The outlet of BLWT is fitted with an axial fan of (diameter 2.8 m), which can provide a maximum wind speed of 20 m·s^{-1}.
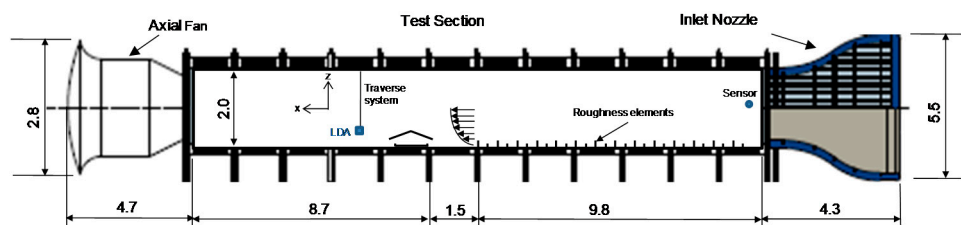

Figure 2. Schematic diagram of Boundary Layer Wind Tunnel (BLWT) (ATB, unpublished) and the experimental setup. All dimensions are in m.

A 1:100 scale model of the NVD building located in north-east Germany was built for the BLWT experiment as described in Figure 1. The dimensions of the scale model are 0.962 m (length) × 0.342 m (width). The eave height and the ridge height are 0.042 m and 0.107 m, respectively (Figure 3a). This resulted in a wind tunnel blockage ratio of 1.72%, which is lower than the recommended maximum value of 5% for scaled model and wind tunnel experiments [24]. The inflow profile was fulfilled the criteria for a boundary layer over a moderately rough terrain according to the VDI guideline for Physical Modelling of Flow and Dispersion Processes in the Atmospheric Boundary Layer [25]. With the barn model height as characteristic length and the local velocities at the barn, a Reynolds number of ~37.000 was achieved for the inside flow of the model, which is published in a previous study with the same model [26]. This meets the requirements of the internal Reynolds number independence on the flow within the model [27], making the wind tunnel results up scalable.
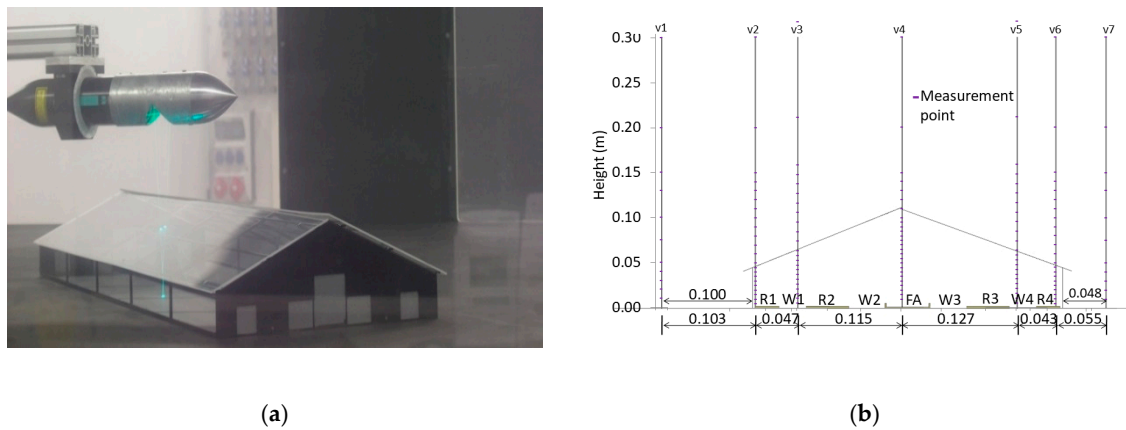
Figure 3. (**a**) A 1: 100 scale model of the NVD building inside BLWT and (**b**) Measurement points in and outside of the NVD barn. R—Cow resting area, W—Cow walking area, and FA—Feeding alley. All dimensions are in m.

No interior partitions except elevated cow resting areas and a feeding alley were constructed in the scale model. The walls and roofs were made of transparent acrylic glasses (2 mm thickness) and were fixed onto the frame using smooth adhesive.

2.2.2. Experimental Setup

The scale model of the NVD building with complete sidewall open was placed along the symmetry line of the wind tunnel with a distance of 11.3 m from the inlet of the BLWT (Figure 2). Sidewall openings of the scale model were perpendicular to the wind direction. The wind tunnel inlet wind speed was 8 m·s^{-1} during measurements since with this wind speed fully developed turbulent flow can be obtained in the wind tunnel [28]. The air velocity profiles in a vertical direction were measured in different locations in and outside of the NVD barn (Figure 3).

Air velocities inside and around the scale model were measured using a 2D Laser Doppler Anemometer (LDA) (Dantec Dynamics, Skovlunde, Denmark). At every measurement point, time series of the air velocity component U (in stream-wise direction) and the wind velocity component V (in span-wise direction) were recorded. Each measurement point was measured until the standard deviation of the average value showed less than 2% fluctuations. Dependent on the sampling rate, this was achieved in a duration approximately between 1.5 and 10 min. At the upstream end of the test section, the mean stream-wise air velocity profile within the BLWT followed a power law Equation (1):

$$U_z = U_{ref}\left(\frac{Z}{Z_{ref}}\right)^{\alpha} \tag{1}$$

where U_z is the wind speed at the height Z; U_{ref} is the reference wind speed at the standard height Z_{ref}, Z_{ref} is the referred standard height 0.1 m (i.e., approximate height of the scale model) was used in the experiment. The U_{ref} = 4.41 m·s^{-1} at Z_{ref} of 0.1 m. The power law exponent of the turbulent boundary layer $\alpha = 0.16$ was determined from the wind tunnel experiment (Figure 4a) without any scale model. Meanwhile, the turbulence intensity profile was also determined Equation (2) which fit best to an exponential law ($R^2 = 0.989$) (Figure 4b).

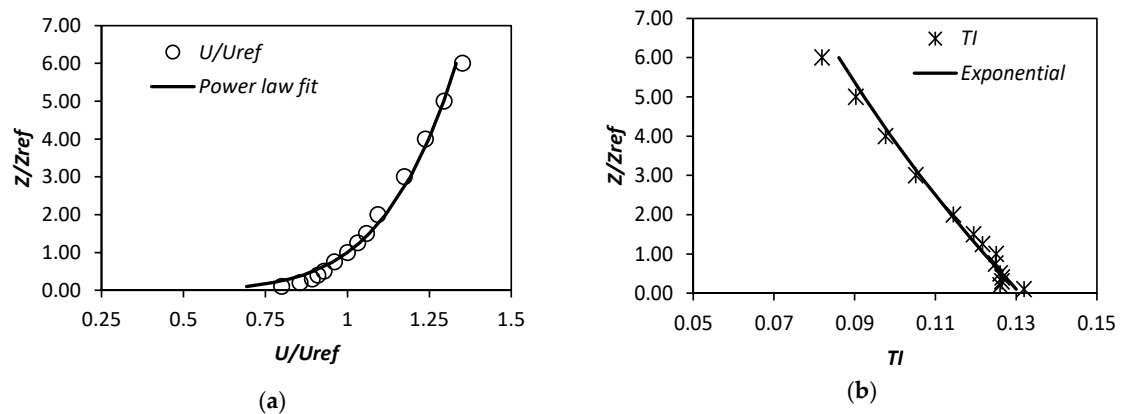$$TI = 0.131exp^{-0.07\left(\frac{Z}{Z_{ref}}\right)} \tag{2}$$

Figure 4. (**a**) Non-dimensional air velocity and (**b**) turbulence intensity profiles of the incident airflow inside wind tunnel.

2.3. CFD Simulations

2.3.1. Geometry and Design of Simulation Cases

The size of the geometry of the NVD building (1:100 scale) was based on the wind tunnel experiment as described in Section 2.2.1. A simplified building geometry was used for the CFD simulation without considering interior partitions except elevated cow resting areas and feeding alley. This is because previous research has shown that a high level of detail in the CFD model would not influence the overall airflow inside the room but significantly increase grid and computational cost [29].

The air flow in the wind tunnel can be modeled using the laws of conservation of mass and momentum (i.e., the Navier Stokes equation). The construction of the building geometry and the mesh were done by ANSYS ICEM CFD in ANSYS Workbench 2019 R2 platform (ANSYS Inc). Eight opening scenarios (Table 1) were generated for the CFD study where SM (only middle part is open) and SMBD (middle and bottom parts of side walls and doors open) scenarios were similar to the field practices (Figure 1a,b). The SWC scenario (Figure 5) i.e., Case 4 was similar to the experiment in the BLWT based scale model (Figure 2) studies and also chosen for CFD model validation. Other seven opening scenarios were studied using the CFD simulations to investigate airflow patterns and find better opening control strategies considering local airflow conditions in steady state condition.

Table 1. Description of computational fluid dynamics (CFD) simulation cases. Cases 1 to 8 are the cases with eight opening combinations (as described in Figure 5) of NVD building using the wind tunnel inlet velocity of 8 m·s^{-1}. Cases 9 to 18 are the cases with ten wind speeds with a constant opening configuration (i.e., SM-Middle part of side walls open).

Cases	Opening Combination	U at WT Inlet (m·s^{-1})	A_{inlet} (m^2)	A_{outlet} (m^2)	A_{roof} (m^2)	A_{doors} (m^2)	A_{fa} (m^2)	$\sum A_{outlet}$ (m^2)
Case 1	SM	8	0.019	0.019	0.002			0.021
Case 2	SMT	8	0.031	0.031	0.002			0.033
Case 3	SMB	8	0.032	0.032	0.002			0.034
Case 4	SWC	8	0.043	0.043	0.002			0.045
Case 5	SWFD	8	0.043	0.043	0.002		0.004	0.049
Case 6	SMTD	8	0.031	0.031	0.002	0.012		0.045
Case 7	SMBD	8	0.032	0.032	0.002	0.012		0.046
Case 8	SWCD	8	0.043	0.043	0.002	0.012		0.057
Case 9	SM	1	0.019	0.019	0.002			0.021

<div align="center">**Table 1.** *Cont.*</div>

Cases	Opening Combination	U at WT Inlet (m·s^{-1})	A$_{inlet}$ (m^2)	A$_{outlet}$ (m^2)	A$_{roof}$ (m^2)	A$_{doors}$ (m^2)	A$_{fa}$ (m^2)	$\sum$A$_{outlet}$ (m^2)
Case 10	SM	2	0.019	0.019	0.002			0.021
Case 11	SM	3	0.019	0.019	0.002			0.021
Case 12	SM	4	0.019	0.019	0.002			0.021
Case 13	SM	5	0.019	0.019	0.002			0.021
Case 14	SM	6	0.019	0.019	0.002			0.021
Case 15	SM	7	0.019	0.019	0.002			0.021
Case 16	SM	8	0.019	0.019	0.002			0.021
Case 17	SM	9	0.019	0.019	0.002			0.021
Case 18	SM	10	0.019	0.019	0.002			0.021

Case 1 SM

(Middle part of side walls open)

Case 5 SWFD

(Complete side walls and feeding alley doors open)

Case 2 SMT

(Middle and top parts of side walls open)

Case 6 SMTD

(Middle and top parts of side walls and doors open)

Case 3 SMB

(Middle and bottom parts of side walls open)

Case 7 SMBD

(Middle and bottom parts of side walls and doors open)

Case 4 SWC

(Complete open side walls)

Case 8 SWCD

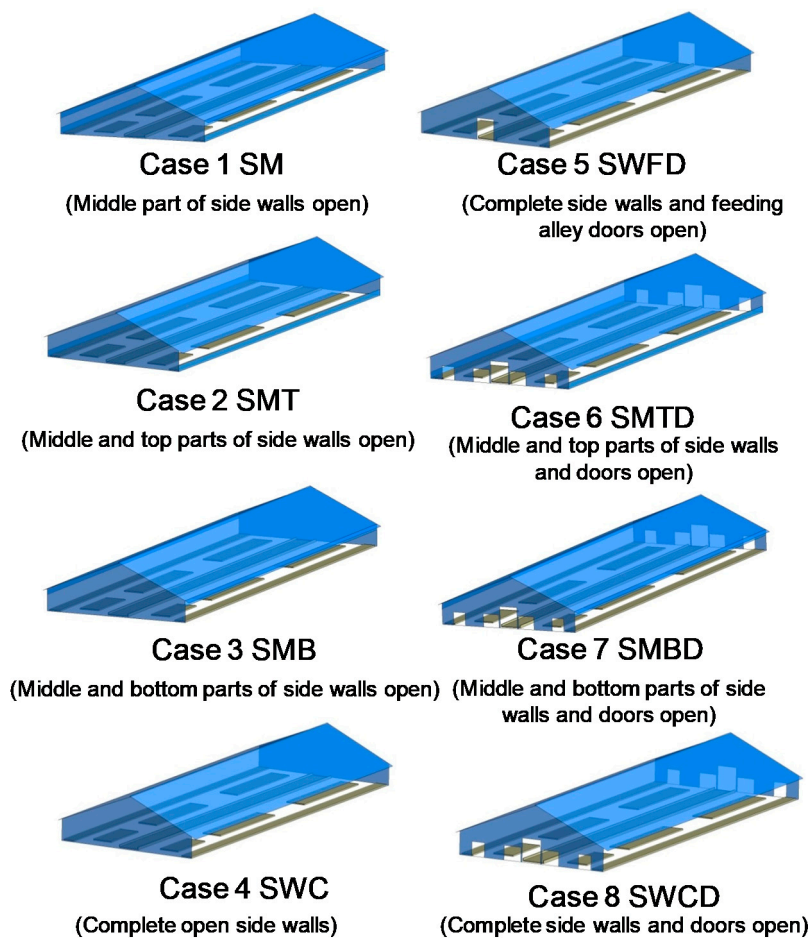(Complete side walls and doors open)

Figure 5. Eight cases with different geometrical opening scenarios of an NVD barn. The roof opening was kept open in all cases.

2.3.2. Model Set Up and Boundary Conditions in CFD

The steady state conditions were used in the CFD analysis of the single-phase airflow in the domain. The computational domain in this study had the dimension of L × W × H = 5.06 m × 6.06 m × 2.03 m. The distances from the scale model to the inlet, outlet, side walls (i.e., parallel to airflow), and the top of the domain were almost 19H$_1$ (H$_1$ = 0.107 m, height of the building), 24H$_1$, 23H$_1$, and 17H$_1$, respectively. It was recommended that the distance from the building to the inlet, to the sides, and to the top of the domain shall be at least five times the building height and the distance from the building to the outlet at least fifteen times the building height [23]. Because the boundaries of the computational

domain should be far enough away from the region of interest, and in our study, distances from each side from the region of interest were far bigger than the recommended minimum. These distances were chosen intentionally for studying the effects of surroundings and wind direction in the future study. Even though it would cost more meshes and calculation time, there will not be any sidewalls effect on the airflow.

Velocity inlet was used for upstream boundary condition. The inlet air velocity profile was calculated by Equation (1) using the same reference value U_{ref} and Z_{ref} as the wind tunnel experiment, which represents boundary layer airflow for an open field. The turbulence intensity profile of the wind tunnel was followed the Equation (2). Turbulent intensity (fraction value) profile was assigned with an expression (ANSYS CFX) following Equation (2) along with turbulence length scale of 0.05 m; roughly representing the height of roughness elements in the BLWT. Wall boundary was used for the walls of the scale model, and the top and the sides of the computational domain. The sand grain roughness height of 2.5×10^{-4} m was used for the ground surface in the direct vicinity of the scale model, which was equivalent to the surface roughness of the wind tunnel. The top of the computational domain was modeled as a free slip wall (zero normal velocity and zero normal gradients of all variables). The other wall boundaries were set as a no-slip smooth wall. Pressure outlet with zero static pressure was imposed at the outlet boundary.

For various wind speed investigations, the inlet velocity U was set to 1, 2, 3, 4, 5, 6, 7, 8, 9, and 10·m·s^{-1}, respectively for a single opening scenario (Case 1, Table 1). Eight opening scenarios and 10 velocities resulted in a total number of 18 simulations. The effect of different opening scenarios (Table 1) on airflow pattern and airflow rate were simulated and investigated using the wind tunnel inlet velocity 8 m·s^{-1} which is correspondence the reference velocity U_{ref} 4.41 m·s^{-1}. The other boundary conditions remained the same as described before.

2.3.3. Numerical Method

For isothermal calculation, the CFD is the solution of transport equations for the conservation of mass and momentum. Finite volume approach was adopted in this study by the commercial code ANSYS CFX 20119 R2 (ANSYS Inc). The standard k-ε turbulence model was chosen for good results accuracy with the robustness of the solution [17,29–31]. Only isothermal simulations are performed in this study in line with the boundary layer wind tunnel (BLWT) measurements. The SIMPLE algorithm was used for the pressure velocity coupling. For the discretization of the convective term, the 2nd order upwind scheme was employed. The solutions were considered to be converged when the residuals of continuity, momentum, and turbulence were small than 1×10^{-5} and when there was no obvious change of the average velocity at the center of the building. The eight sidewall opening scenarios (Figure 5) were simulated using the same boundary settings.

2.3.4. Grid Details and Grid Independence Study

The computational domain was discretized using ANSYS ICEM CFD (ANSYS Workbench 2019 R2) by structural hexahedral cells with lower densities allocated at outer boundaries and higher densities distributed around and within the building model where steep velocity gradient occurs. The optimal grid distribution of the computational domain with 1:100 scale model of NVD building in and around is shown in Figure 6a,b.

Grid independence was analyzed to ensure that the resolution of the mesh did not influence the results by using three different density grids (867,082, 2,345,564, and 4,885,144 cells, respectively) (Figure 7a,b). The optimum grid distribution was achieved by completing a grid-independence control at the inlet boundary velocity of 4 m·s^{-1}, during which three different simulations were run with different meshes, until the velocity distribution was constant for the specific point.
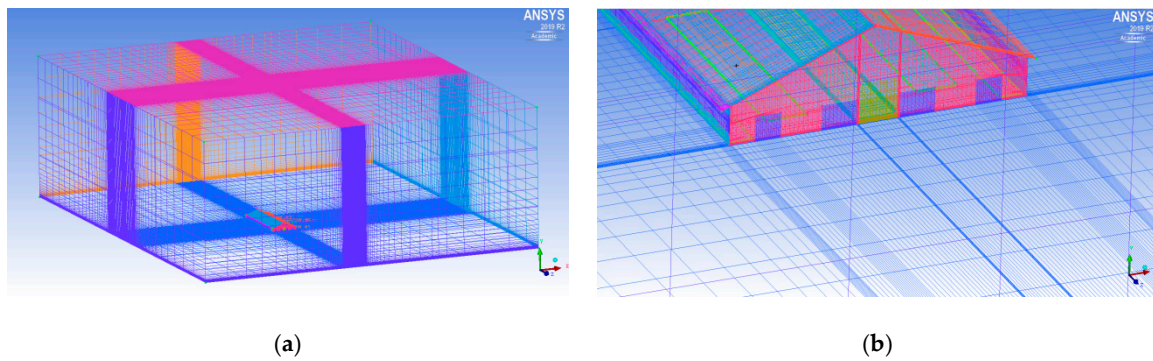
Figure 6. Grid distribution in the computational domain and at the building surfaces. (**a**) iso-metric view of the whole computational domain and (**b**) iso-metric view closed to the model.
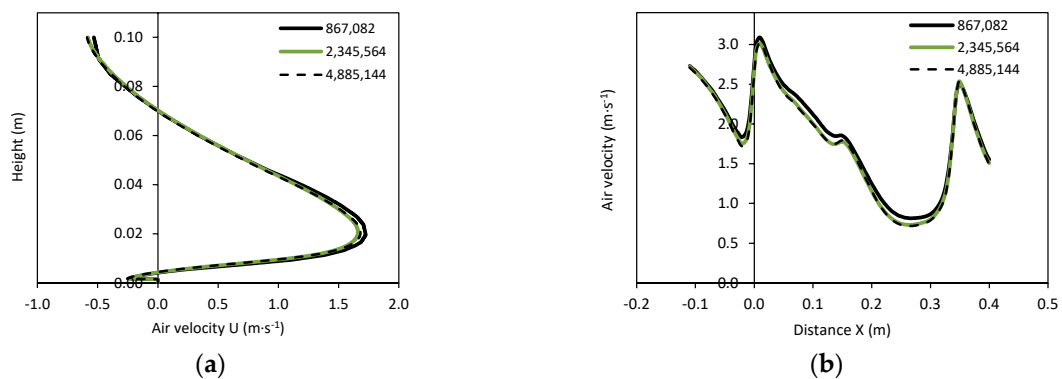

Figure 7. A grid independency study with three density grids. (**a**) vertical profile, and (**b**) horizontal profile inside middle of the NVD barn with SM opening conditions.

Figure 7 shows the results of the grid independence study. The vertical U velocity profile at the center (x = 0.165 m, y = 0.478 m) of the NVD barn, and the horizontal U velocity profile at the 0.02 m height started from 0.015 m from the windward side sidewall and ended after 0.05 m of the leeward side of the NVD building were compared. There was a slight difference (max difference 0.146 m·s^{-1}) between the solutions of the medium and low density meshes, while no considerable differences between medium and high density meshes were observed. Therefore, in this study, the medium density mesh (2,345,564 cells) was used for further simulation.

2.4. CFD Model Validation

The air velocities along seven vertical lines for the Case 4 SWC (Summer case, Figure 1a) obtained from wind tunnel experiments and CFD simulations were compared for validating the CFD model (Figure 8). The CFD simulations reasonably revealed the characteristics of the measured velocity in terms of airflow pattern and magnitudes (Figure 8). However, there are slight discrepancies inline v2 (close to inlet wall) and v4 (inside feeding alley) between simulated and measured velocity. Small deviations were observed above the roof of the leeward side for line v5 and v6. One explanation could be that uncertainty might exist for the LDA precisely located at the specific measurement positions just after the inlet side wall and inside the feeding alley, although much attention was paid to it. However, weakness of the RANS models in predicting the air separation might also be the cause [17,32]. Even though there were small discrepancies between the experiment and the simulation, the results indicated that the CFD model is feasible for modeling airflow characteristics in the naturally ventilated building as airflow in and outside the scale model followed similar trends in simulation as BLWT experimental results. Therefore, further simulations were conducted for all the cases following the similar set-up and model in CFD.
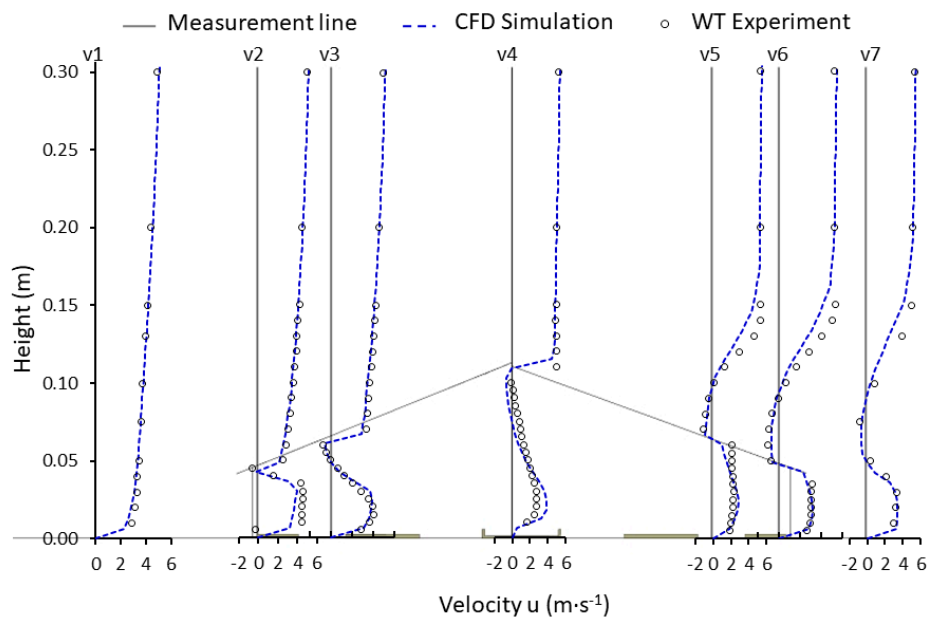
Figure 8. Comparison of stream-wise air velocity (*u*) profiles of BLWT measurement data with CFD simulation in different locations in and outside of the NVD barn for the completed opened sidewalls condition (Case 4 SWC). The inlet profile velocity at 0.1m height was 4.41 m·s^{-1}. The zero velocity in x axis correspondence with the line of the measurement. Negative value of the velocity indicates opposite direction of airflow.

2.5. Calculation of Airflow Rate and Non-dimensional Airflow Rate

The airflow rate (*Q*) was calculated in different openings by summing the partial airflow rates through the cell faces of the windward opening:

$$Q = \sum_{i \in N} U_i A_i \tag{3}$$

where N is the cell number of the windward opening, U_i is the stream-wise air velocity through cell i, m·s^{-1}, and A_i is the face area of cell i, m^2.

Non-dimensional airflow rate was calculated using Equation (4).

$$Q^* = \frac{Q}{U_{ref}.A_{in}} \tag{4}$$

where Q^* is the non-dimensional airflow rate; U_{ref} is the reference velocity at 0.1 m height, m·s^{-1}; A_{in} is the area of the windward sidewall opening, m^2. However, the calculation of the non-dimensional airflow rate of other openings were calculated using same approach where the area of openings were only different.

Airflow rate per m^2 floor area (Q_f) was calculated considering airflow rate and floor area of the NVD building as Equation (5).

$$Q_f = \frac{Q}{A_f} \tag{5}$$

where *Q* is the airflow rate through the windward opening, m^3·s^{-1}, and A_f indicates the floor area of the building.

3. Results and Discussion

3.1. Airflow Characteristics in and outside the NVD Building

Figure 9 shows the steady state simulation results of airflow streamlines inside and around the NVD building for different opening combinations. Different airflow patterns were observed for different opening scenarios at the same reference wind speed (U_{ref} = 4.41 m·s^{-1}) which correspondence to inlet velocity 8 m·s^{-1}. In all the cases, when the wind approached the building, most of the airstreams entered the building via the windward opening. The major part of the airflow stream either attached to the floor (Case 1, Case 3 to 5, and Case 7 to 8) or attached to the ceiling (Case 2 and 6) before leaving the leeward sidewall opening. A small portion of the airflow stream directly flowed out through the roof opening. The remaining air streams re-circulated either close to the floor (Case 2 and Case 6) or attached to the ceiling (Case 1, Case 3 to 5, and Case 7 to 8), created vortex and passed through sidewall and roof openings.
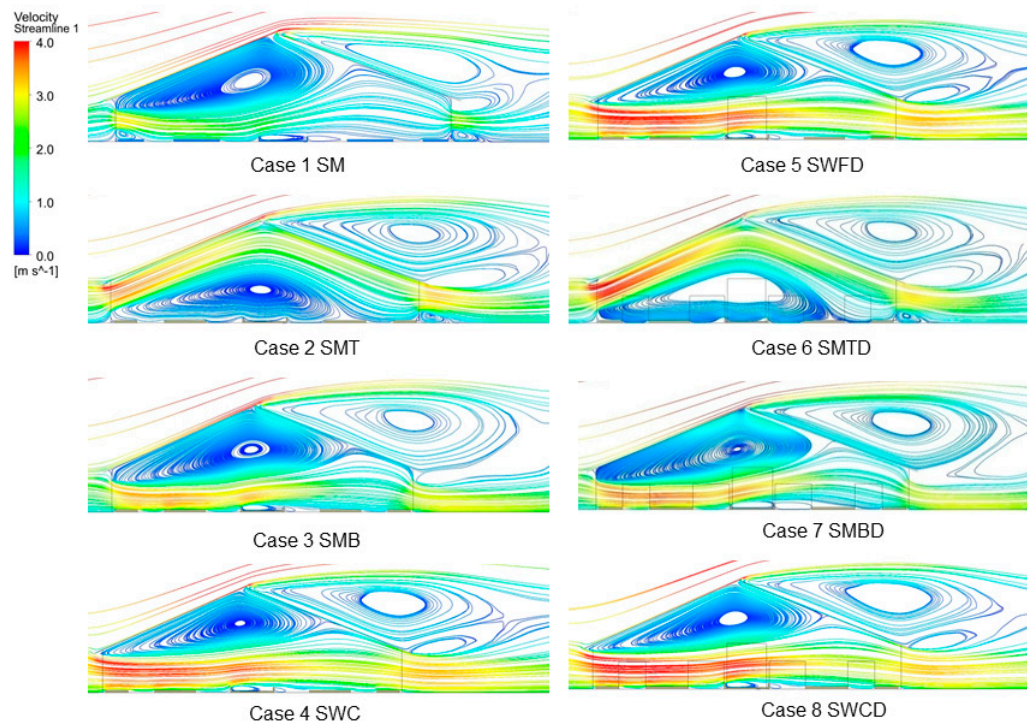

Figure 9. Airflow patterns inside and outside of the NVD barn for different opening combinations. The inlet velocity followed the profile described by Equation (1), and the reference profile velocity was 4.41 m·s^{-1} at the height of 0.1 m.

For Case 1 SM with the middle part of both side walls opened, which is the case for the spring and autumn opening practices in the research barn Dummerstorf, the major jet approached directly towards the middle animal resting place (R2, as location shown in Figure 3b) while a small jet formed a vortex above the first animal resting place (R1, as location shown in Figure 3b). After passing above the resting places (R1, R2) and animal walking alley, major jet diverted at the wall of windward side of the feeding alley (FA, as location shown in Figure 3b). Then the air velocity became weaker when it touched the animal resting floors and walking alleys before leaving the leeward opening. This indicated that animals staying at the leeward side of the feeding alley may have less fresh air than those staying at the windward side. However, the animal comfort will be different depending on the jet of cold air [4] or warm air [33]. The small or weaker jets which could not go through roof opening created a recirculation zone below the windward roof. As seen from Figure 10, this vortex became smaller as the

approached wind became stronger. It is also found that the higher the wind speed approached the building, the higher the velocity of the jet entering the building. There was creation of recirculation zone just after the feeding alley (Cases 14 to 18). Additionally, a vortex formed above the leeward roof in all cases (Figures 9 and 10) though the size of the vortex depended on the approach wind speed and different opening combinations.
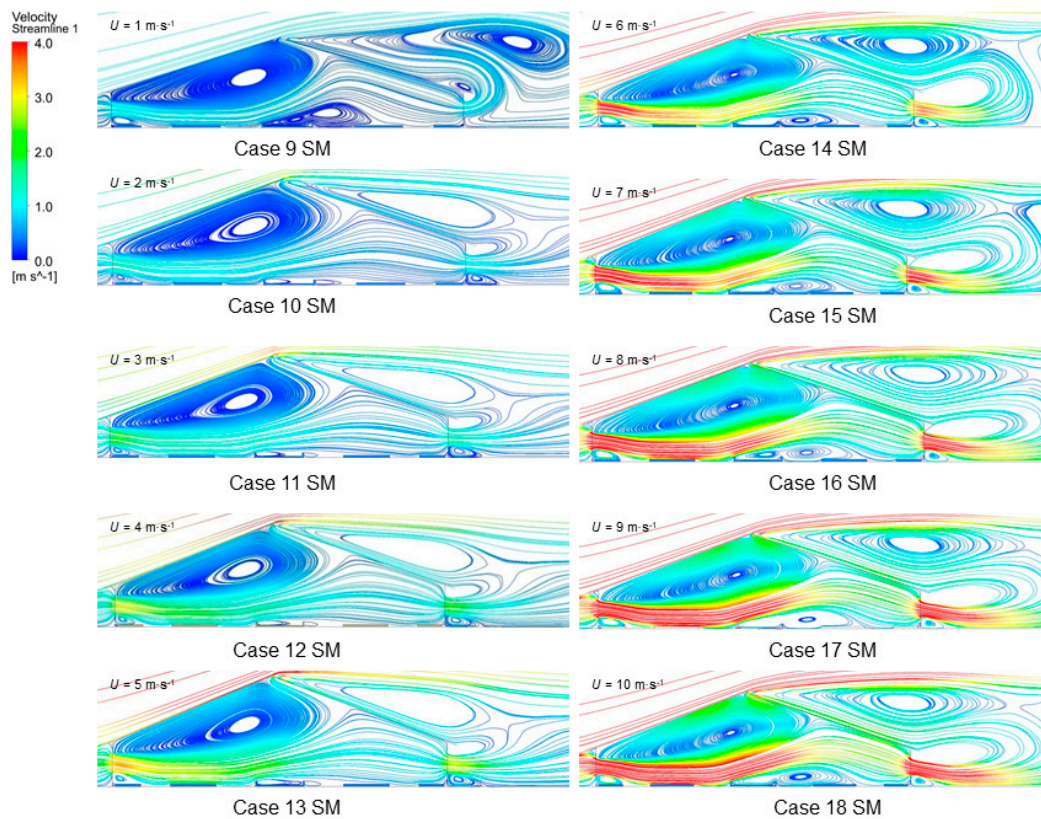

Figure 10. Airflow patterns inside and outside of the NVD barn for the inlet velocity of 1 to 10 m·s^{-1}. SM—Middle part of the sidewall is open.

In Case 2 SMT and Case 6 SMTB (Figure 9), the incoming air flowed upwards immediately after passing through the windward opening, and the air recirculation region consisted of low air velocities formed above the floor. This is probably caused by the bottom sidewalls that acted as guiding plates of airflows. The similar up-jet airflow pattern was also observed by Yi et al. [15] and Morsing et al. [34] in naturally ventilated livestock barns for the cases with high bottom sidewalls.

For the Case 3 SMB and Case 7 SMBD (summer practice in NVD at Dummerstorf), the strong jet attached to cow resting floors and walking alleys more in the windward sides than in the leeward side. The remaining jet circulation phenomenon was same as Case 1 SM except the size of the eddy and jet velocity was stronger above the feeding alley than the Case 1 SM. However, a strong influence on jet diversion by the wall of the feeding alley was found which was not considered in other studies [17,28], even though this diversion became more visible when the approaching wind became stronger (Figure 10).

The jet entering into the building with complete sidewall opens in both the windward and leeward sides was stronger in Case 4 SWC, Case 5 SWFD, and Case 8 SWCD than the other cases in the same velocity of approached wind (Figure 9). The airflow pattern was the same in Cases 4, 5, and 8 but with slightly higher incoming air velocities in Case 8. This was caused by the opened doors that increased the incoming jet momentum. It indicated that the doors on gable walls had influences on indoor air velocities, which may affect cow comfort and gaseous emissions.

3.2. Air Velocity at the Animal Height and Just above the Emission Surface

Figure 11a shows air velocities at the cow height in different locations for Cases 1 to 9. Large variations in local air velocities were observed with different opening combinations. In most areas, the highest air velocities at the cow height occurred in Case 8 SWCD, where both sidewalls and all gates were completely open. In locations near the windward side i.e., R2, W2, FA, the highest air velocities were observed in Case 3 SMB, where the practical opening configuration is used in summer. By contrast, Case 2 SMT gave the lowest air velocities at the cow height except in the region near the leeward side where the lowest air velocities happened in Case 6 SMTD and Case 7 SMBD. This was probably caused by the up-jet airflow pattern with air recirculation zone positioned near the floor, as seen in Figure 9. In addition, it was found that the closer to the windward side, the higher the air velocities at the cow height. Similar results were found in Yi et al. [14] 1:40 scale model study. It indicated non-uniform airflow distributions in the animal occupied zone with likely better ventilation in the windward side than in the leeward side.
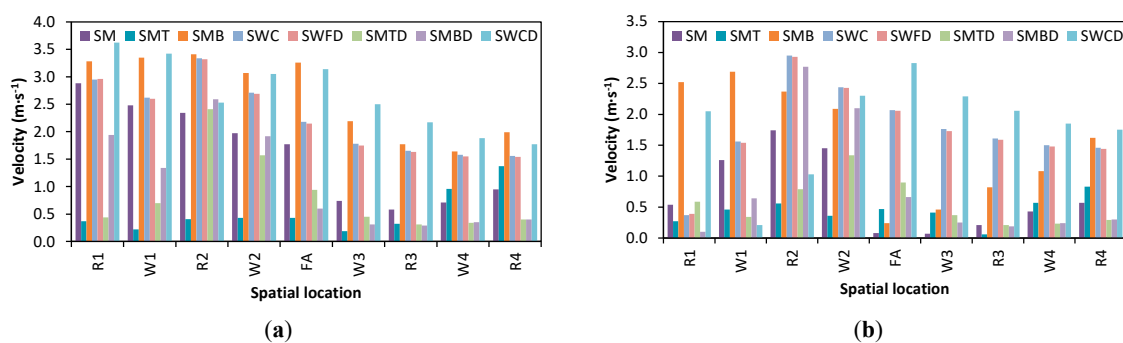

Figure 11. Effects of different opening combinations on air velocities in different locations away from the windward side at the middle of the barn (**a**) at the cow height and (**b**) close to the emission surface. R—Cow resting area, W—Cow walking area and FA—Feeding alley.

The air velocities close to the emission surface in different locations and different opening combinations are compared in Figure 11b since the ammonia release is closely related to the air velocity over the manure surface [35]. Generally, the highest air velocities occurred at the locations W1 and R2, from where the most ammonia emissions would be released because of an increased convective mass transfer coefficient, but the amount of manure soiling the floor is an important factor of ammonia emission. Case 3 SMB and Case 8 SWCD contributed to higher air velocities above the emission surface near the windward side and near the leeward side, respectively, and thus higher ammonia emissions from the barn. Increasing air velocity effects on increasing ammonia emissions [1,36,37] because ammonia evaporation losses increased linearly with the increasing airflow velocities at the floor level [38,39]. By contrast, Case 1 SM opening configuration tended to give lower near floor air velocities which may result lower emissions, especially in the middle and near the leeward side of the barn. The results indicated that the opening combination may affects cow comfort depending on the location of the cows, and the emission. Therefore, the seasonal opening combinations can be controlled depending on the outside weather conditions.

3.3. Airflow Rate

The airflow rate per m^2 floor area (Q_f) was calculated using the ventilation rate divided by the area of the building. The Q_f of the NVD building increased with the increase of the external air velocity. Compared with the SM opening combination, the Q_f was 1.92, 1.57, 2.39, 2.41, 2.01, 1.66, and 2.45 times higher in SMT, SMB, SWC, SWFD, SWTD, SMBD, and SWCD opening combinations, respectively. Larger openings resulted in higher Q_f than smaller openings (Figure 12), which is in line with the study of De Paepe et al. [22]. The Q_f of SMT is greater than SMB even though they have the same opening areas. However, the opening location of SMT is higher than SMB, which has larger air

velocities through the windward opening and thus a higher Q_f. Door openings in gable walls also had some influences on the Q_f even though the wind direction was perpendicular to sidewall openings. For example, the Q_f of SWFD is 0.8% higher than SWC, which is caused by the door opening in the feeding alley. The Q_f of SWCD is 2.5% higher than SWC when all doors were open. The highest Q_f was obtained in SWCD case where generally the highest air velocities occurred at the animal height and near the emitting surface.
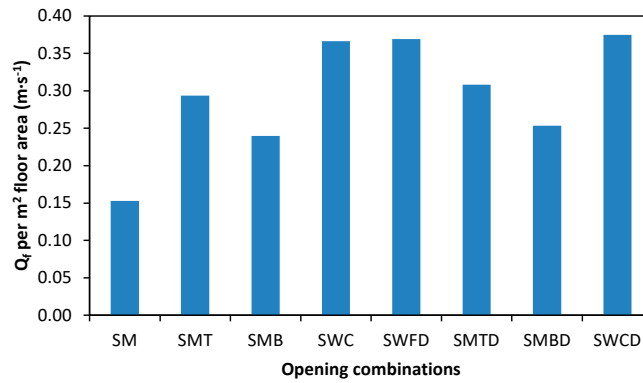
Figure 12. Airflow rate per unit floor area in different opening combinations.

Figure 13 shows the non-dimensional ventilation rate (Q^*) through different openings in different cases. The highest ventilation occurred through the windward sidewall opening, followed by the leeward opening in all cases. The roof opening and doors contributed to only a small part of the ventilation rate compared with sidewall openings. The perpendicular wind direction is the main reason for this phenomenon. The Q^* through the windward sidewall opening in SMT and SMTD opening configurations were obviously higher than the rest cases. It was partly caused by the boundary layer wind profile with higher air velocities occurring at a higher altitude.
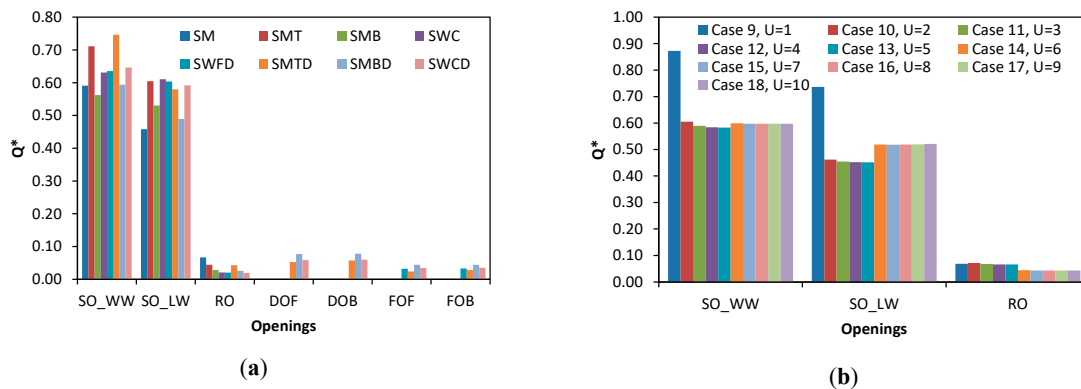

(a)

(b)

Figure 13. Non-dimensional airflow rate (Q^*) at the different openings of NVD building for (**a**) Case 1 to Case 8 with same reference velocity U_{ref} = 4.41 m·s^{-1} and (**b**) Case 9 to Case 18 for different inlet velocity (U) 1 to 10 m·s^{-1}; where SO_WW—Side wall opening in windward side, SO_LW—Sidewall opening at leeward side, RO—Roof opening, DOF—Doors opening in the front gable wall, DOB—Doors opening in the back gable wall, FOF—Feeding alley opening in the front gable wall, and FOB—Feeding alley opening in the back gable wall. U value in the legend indicates inlet velocity in m·s^{-1}.

The presence of the bottom sidewall was another possible reason since it guided the air flow upwards which increased the air velocities through the windward opening. The results indicated that the control of the ventilation rate mainly depends on the control of sidewall openings, while the effects from the ridge opening and doors are minimal in the perpendicular wind direction and wind-driven ventilation conditions. In addition, it was found that when the inlet air velocity increased over 6 m·s⁻¹, the $Q*$ through the leeward opening increased dramatically. Under this circumstance, the airflows tended to leave the building via the leeward opening than via the roof opening.

4. Conclusions

This paper brings detailed insight into distribution of airflow at the animal height and near the emission surface as well as airflow characteristics in a scale model of a naturally ventilated dairy building. Computational fluid dynamics (CFD) simulations of air velocity profiles using the standard k-ε model reasonably agreed with the measurements for a 1:100 scale model of a naturally ventilated dairy building inside a large BLWT. Different airflow patterns were observed and airflow rates were calculated under different opening combinations and wind speed conditions using the experimentally validated CFD modelling technique. The conclusions drawn from this study are summarized as follows:

- Opening combinations play a decisive role in the distribution of fresh air inside the barn. Complete sidewall opening either with door or feeding alley openings in both leeward and windward sides showed better distribution of airflow in the summer season. In Autumn, when the middle part of the sidewall opens, after passing above the resting places and animal walking alley of windward side, major jet diverted at the wall of windward side of the feeding alley. Due to feeding alley wall, the air velocity became weaker when it touched the animal resting floors and walking alleys before leaving the leeward opening. This indicated that animals staying at the leeward side of the feeding alley may have less fresh air than those staying at the windward side.
- Inlet air can be guided by sidewall openings depending on seasonal ambient air temperatures for animal comfort and minimal emission. When opening of the bottom part of the sidewall contributed increased air velocities near emission surfaces. Therefore, the bottom part of the sidewall should not be opened until the cow comfort hampers due to hot summer.
- Different opening combinations showed that airflow rate per m² floor area was 1 to 2.5 times higher than when only middle part of the sidewall was opened. Larger sidewall openings resulted in higher airflow rate than the small openings while the effect from ridge opening and door opening were minimal in the perpendicular wind direction.

Further studies are required to understand wind directions and surroundings effect on the airflow pattern and airflow rate of NVD buildings. Non-isothermal and transient simulations of NVD buildings should be carried out for better understanding of airflow patterns and airflow exchange rate. Further studies are needed to investigate the non-isothermal case with cows and feedstock inside the NVD building. Sensor-based opening control can be introduced in combination with CFD simulation in the near future for better management of airflow.

References

1. Saha, C.K.; Zhang, G.; Ni, J.Q. Airflow and concentration characterisation and ammonia mass transfer modelling in wind tunnel studies. *Biosyst. Eng.* **2010**. [CrossRef]

2. Bull, K.R.; Sutton, M.A. Critical loads and the relevance of ammonia to an effects-based nitrogen protocol. *Atmos. Environ.* **1998**, *32*, 565–572. [CrossRef]

3. Samer, M.; Fiedler, M.; Müller, H.J.; Gläser, M.; Ammon, C.; Berg, W.; Sanftleben, P.; Brunsch, R. Winter measurements of air exchange rates using tracer gas technique and quantification of gaseous emissions from a naturally ventilated dairy barn. *Appl. Eng. Agric.* **2011**, *27*, 1015–1025. [CrossRef]

4. Ikeguchi, A.; Zhang, G.; Okushima, L.; Bennetsen, J.C. Windward windbreak effects on airflow in and around a scale model of a naturally ventilated pig barn. *Trans. ASAE* **2013**. [CrossRef]

5. Heinicke, J.; Ibscher, S.; Belik, V.; Amon, T. Cow individual activity response to the accumulation of heat load duration. *J. Therm. Biol.* **2019**, *82*, 23–32. [CrossRef]

6. Smith, J.F.; Bradford, B.J.; Harner, J.P.; Potts, J.C.; Allen, J.D.; Overton, M.W.; Ortiz, X.A.; Collier, R.J. Short communication: Effect of cross ventilation with or without evaporative pads on core body temperature and resting time of lactating cows. *J. Dairy Sci.* **2016**. [CrossRef]

7. Van Buggenhout, S.; Van Brecht, A.; Eren Özcan, S.; Vranken, E.; Van Malcot, W.; Berckmans, D. Influence of sampling positions on accuracy of tracer gas measurements in ventilated spaces. *Biosyst. Eng.* **2009**, *104*, 216–223. [CrossRef]

8. Samer, M.; Loebsin, C.; Fiedler, M.; Ammon, C.; Berg, W.; Sanftleben, P.; Brunsch, R. Heat balance and tracer gas technique for airflow rates measurement and gaseous emissions quantification in naturally ventilated livestock buildings. *Energy Build.* **2011**. [CrossRef]

9. Saha, C.K.; Ammon, C.; Berg, W.; Loebsin, C.; Fiedler, M.; Brunsch, R.; Von Bobrutzki, K. The effect of external wind speed and direction on sampling point concentrations, air change rate and emissions from a naturally ventilated dairy building. *Biosyst. Eng.* **2013**, *114*. [CrossRef]

10. Samer, M.; Ammon, C.; Loebsin, C.; Fiedler, M.; Berg, W.; Sanftleben, P.; Brunsch, R. Moisture balance and tracer gas technique for ventilation rates measurement and greenhouse gases and ammonia emissions quantification in naturally ventilated buildings. *Build. Environ.* **2012**. [CrossRef]

11. Fiedler, M.; Berg, W.; Ammon, C.; Loebsin, C.; Sanftleben, P.; Samer, M.; von Bobrutzki, K.; Kiwan, A.; Saha, C.K. Air velocity measurements using ultrasonic anemometers in the animal zone of a naturally ventilated dairy barn. *Biosyst. Eng.* **2013**. [CrossRef]

12. Snell, H.G.J.; Seipelt, F.; Van Den Weghe, H.F.A. Ventilation rates and gaseous emissions from naturally ventilated dairy houses. *Biosyst. Eng.* **2003**. [CrossRef]

13. Saha, C.K.; Fiedler, M.; Ammon, C.; Berg, W.; Loebsin, C.; Amon, B.; Amon, T. Uncertainty in calculating air exchange rate of naturally ventilated dairy building based on point concentrations. *Environ. Eng. Manag. J.* **2014**, *13*, 2349–2355. [CrossRef]

14. Yi, Q.; König, M.; Janke, D.; Hempel, S.; Zhang, G.; Amon, B.; Amon, T. Wind tunnel investigations of sidewall opening effects on indoor airflows of a cross-ventilated dairy building. *Energy Build.* **2018**. [CrossRef]

15. Yi, Q.; Zhang, G.; König, M.; Janke, D.; Hempel, S.; Amon, T. Investigation of discharge coefficient for wind-driven naturally ventilated dairy barns. *Energy Build.* **2018**, *165*, 132–140. [CrossRef]

16. Norton, T.; Sun, D.W.; Grant, J.; Fallon, R.; Dodd, V. Applications of computational fluid dynamics (CFD) in the modelling and design of ventilation systems in the agricultural industry: A review. *Bioresour. Technol.* **2007**, *98*, 2386–2414. [CrossRef]

17. Yi, Q.; Li, H.; Wang, X.; Zong, C.; Zhang, G. Numerical investigation on the effects of building configuration on discharge coefficient for a cross-ventilated dairy building model. *Biosyst. Eng.* **2019**. [CrossRef]

18. Gebremedhin, K.G.; Wu, B. Simulation of flow field of a ventilated and occupied animal space with different inlet and outlet conditions. *J. Therm. Biol.* **2005**, *30*, 343–353. [CrossRef]

19. Norton, T.; Grant, J.; Fallon, R.; Sun, D.W. Optimising the ventilation configuration of naturally ventilated livestock buildings for improved indoor environmental homogeneity. *Build. Environ.* **2010**. [CrossRef]

20. Yi, Q.; Zhang, G.; Li, H.; Wang, X.; Janke, D.; Amon, B.; Hempel, S.; Amon, T. Estimation of opening discharge coefficient of naturally ventilated dairy buildings by response surface methodology. *Comput. Electron. Agric.* **2020**. [CrossRef]

21. Shen, X.; Zhang, G.; Bjerg, B. Investigation of response surface methodology for modelling ventilation rate of a naturally ventilated building. *Build. Environ.* **2012**. [CrossRef]

22. De Paepe, M.; Pieters, J.G.; Cornelis, W.M.; Gabriels, D.; Merci, B.; Demeyer, P. Airflow measurements in and around scale model cattle barns in a wind tunnel: Effect of ventilation opening height. *Biosyst. Eng.* **2012**, *113*, 22–32. [CrossRef]

23. Franke, J.; Hellsten, A.; Schlünzen, H.; Carissimo, B. *Best Practice Guideline for the CFD Simulation of Flows in the Urban Environment*; Cost Office: Brussels, Belgium, 2007; ISBN 3000183124.

24. Barlow, J.B.; Rae, W.H.; Pope, A. *Low-Speed Wind Tunnel Testing*, 3rd ed.; A Wiley-Interscience Publication, John Wiley & Sons: Hoboken, NJ, USA, 1999; ISBN 0471557749.

25. VDI. Guideline 3783/12. In *Physical Modelling of Flow and Dispersion Processes in the Atmospheric Boundary Layer—Application of Wind Tunnels*; Beuth Verlag: Berlin, Germany, 2000; Volume 3783/12.

26. Janke, D.; Caiazzo, A.; Ahmed, N.; Alia, N.; Knoth, O.; Moreau, B.; Wilbrandt, U.; Willink, D.; Amon, T.; John, V. On the feasibility of using open source solvers for the simulation of a turbulent air flow in a dairy barn. *Comput. Electron. Agric.* **2020**. [CrossRef]

27. Cermak, J.E.; Poreh, M.; Peterka, J.A.; Ayad, S.S. Wind tunnel investigations of natural ventilation. *J. Transp. Eng.* **1984**. [CrossRef]

28. Yi, Q.; Wang, X.; Zhang, G.; Li, H.; Janke, D.; Amon, T. Assessing effects of wind speed and wind direction on discharge coefficient of sidewall opening in a dairy building model—A numerical study. *Comput. Electron. Agric.* **2019**. [CrossRef]

29. Hajdukiewicz, M.; Geron, M.; Keane, M.M. Formal calibration methodology for CFD models of naturally ventilated indoor environments. *Build. Environ.* **2013**. [CrossRef]

30. Shen, X.; Zhang, G.; Wu, W.; Bjerg, B. Model-based control of natural ventilation in dairy buildings. *Comput. Electron. Agric.* **2013**. [CrossRef]

31. Wu, W.; Wang, B.; Malkawi, A.; Yoon, N.; Sehovic, Z.; Yan, B. A Method toward Real-Time CFD Modeling for Natural Ventilation. *Fluids* **2018**. [CrossRef]

32. Ntinas, G.K.; Dados, I.N.; Shen, X.; Malamataris, N.A.; Fragos, V.P.; Zhang, G. Characteristics of unsteady flow around two successive rectangular ribs on floor of a wind tunnel. *Eur. J. Mech. B Fluids* **2017**. [CrossRef]

33. Hempel, S.; Menz, C.; Pinto, S.; Galán, E.; Janke, D.; Estellés, F.; Müschner-Siemens, T.; Wang, X.; Heinicke, J.; Zhang, G.; et al. Heat stress risk in European dairy cattle husbandry under different climate change scenarios-uncertainties and potential impacts. *Earth Syst. Dyn.* **2019**, *10*, 859–884. [CrossRef]

34. Morsing, S.; Ikeguchi, A.; Bennetsen, J.C.; Strøm, J.S.; Ravn, P.; Okushima, L. Wind induced isothermal airflow patterns in a scale model of a naturally ventilated swine barn with cathedral ceiling. *Appl. Eng. Agric.* **2002**, *18*, 97–101. [CrossRef]

35. Ni, J. Mechanistic models of ammonia release from liquid manure: A review. *J. Agric. Eng. Res.* **1999**, *72*, 1–17. [CrossRef]

36. Mackay, D.; Yeun, A.T.K. Mass Transfer Coefficient Correlations for Volatilization of Organic Solutes from Water. *Environ. Sci. Technol.* **1983**. [CrossRef] [PubMed]

37. Arogo, J.; Zhang, R.H.; Riskowski, G.L.; Christianson, L.L.; Day, D.L. Mass transfer coefficient of ammonia in liquid swine manure and aqueous solutions. *J. Agric. Eng. Res.* **1999**. [CrossRef]

38. Vlek, P.L.G.; Stumpe, J.M. Effects of Solution Chemistry and Environmental Conditions on Ammonia Volatilization Losses from Aqueous Systems. *Soil Sci. Soc. Am. J.* **1978**. [CrossRef]

39. Saha, C.K.; Zhang, G.; Kai, P. Modeling ammonia mass transfer process from a model pig house based on ventilation characteristics. *Trans. ASABE* **2012**, *55*, 1597–1607. [CrossRef]